Dalton Transactions

Approaching the isotropic spin-ladder regime: Structure and magnetism of all-pyrazine-bridged copper(II)-based antiferromagnetic ladders

Journal:	*Dalton Transactions*
Manuscript ID	DT-ART-12-2021-004219.R2
Article Type:	Paper
Date Submitted by the Author:	18-Feb-2022
Complete List of Authors:	Monroe, Jeffrey; Clark University, Department of Chemistry Carvajal, M.Angels; Universitat de Barcelona, Quimica Fisica Landee, Christopher; Clark University, Department of Physics Deumal, Mercè; Universitat de Barcelona, Quimica Fisica Turnbull, Mark; Clark University, Department of Chemistry Wikaira, Jan; University of Canterbury, Department of Chemistry Dawe, Louise; Memorial University of Newfoundland, Chemistry

Approaching the isotropic spin-ladder regime: Structure and magnetism of all-pyrazine-bridged copper(II)-based antiferromagnetic ladders

Jeffrey C. Monroe,[a,*] M. Angels Carvajal,[b] Christopher P. Landee,[c] Mercè Deumal,[b*] Mark M. Turnbull[a,*] Jan L. Wikaira[d] and Louise N. Dawe[e]

[a]Carlson School of Chemistry and Biochemistry, Clark University 950 Main Street, Worcester MA 01610, USA

[b]Dept. Ciència de Materials i Química Física, & IQCTUB, Universitat de Barcelona, Martí i Franquès 1, Barcelona, E-08028.

[c]Department of Physics, Clark University 950 Main Street, Worcester MA 01610, USA

[d]Department of Chemistry, University of Canterbury, 20 Kirkwood Ave, Upper Riccarton, Christchurch 8041, New Zealand

[e] Dept. of Chemistry and Biochemistry, Wilfrid Laurier University, Waterloo, Ontario, Canada

Abstract:

The crystal structure and magnetic properties of two all-pyrazine-bridged antiferromagnetic spin ladders are reported. The complexes, *catena*-(bis(3-X-4-pyridone)(μ-pyrazine)copper(II)(-μ-pyrazine)diperchlorate ($[Cu(pz)_{1.5}(L)_2](ClO_4)_2$ where L = 3-X-4-pyridone and X = Br (**1**) or Cl (**2**)), contain copper(II)-based ladders in which both the rung and rail bridges are pyrazine molecules bonded through the x^2-y^2 orbital of the copper(II) ions. This structural scaffold is proposed to approach the isotropic spin-ladder regime. **1** and **2** crystallize in the monoclinic space group $P2_1/c$. Due to the bulk of the 3-X-4-HOpy ligands, the ladders are well isolated in the *a*-direction (**1**, 15.6 Å; **2**, 15.5 Å). The ladders, which run in the *b*-direction, are stacked in the *c*-direction with the separation (**1**, 7.87 Å; **2**, 7.82 Å) between copper(II) ions caused by the bulk of a semi-coordinate perchlorate ion coordinated in the axial position. Computational evaluation of magnetic J_{AB} couplings between Cu-moieties of **2** supports the experimentally proposed magnetic topology and agrees with an isolated isotropic spin-ladder (J_{rail} = -4.04 cm^{-1} (-5.77 K) and J_{rung} = -3.89 cm^{-1} (-5.56 K)). These complexes introduce a convenient scaffold for synthesizing isotropic spin-ladders with modest superexchange interactions, the strength of which may be tuned by variations in L. The magnetic susceptibility down to 1.8 K, for both compounds, is well described by the strong-rung ladder model giving nearly isotropic exchange with $J_{rung} \approx J_{rail} \approx$ -5.5 K (**1**) and -5.9 K (**2**) using the $\hat{H} = -2\sum_{(A,B)} J_{AB}\hat{S}_A \cdot \hat{S}_B$ Hamiltonian. Theoretical simulations of the magnetic response of **2** using the isotropic ladder model are in excellent agreement with experiment. The measured magnetization to 5 T

indicates a quantum-dominated magnetic spectrum. Again, calculated lower and saturation (4.3 and 24 T, respectively) critical fields for **2** are consistent with experimental measurements, and magnetization data at very low temperatures indeed suggest the presence of quantum effects. Further, the computational study of short- and long-range spin ordering indicates that a 2D-to-3D crossover might be feasible at lower temperatures. Analysis of the Boltzmann population corroborates the presence of accessible triplet states above the singlet ground state enabling the aforementioned 2D-to-3D crossover.

Introduction:

Spin ladder systems have been of interest since theoretical predictions intended to describe the low-dimensional magnetic behavior of some potentially superconducting copper-oxide compounds revealed a rich magnetic excitation spectrum.[1,2,3] The synthesis of copper(II) molecular lattices comprising ladders has since been pursued[4,5,6,7] as weakly interacting analogs enabling field dependent investigations of the magnetic spectrum, ideally to saturation in an applied field of < 20 T. These molecular systems have provided insightful probes into the ladder phase diagram as a function of the exchange strengths within the ladders and between ladders.[8,9,10,11,12]

Chemists have, over the decades, developed experimental scaffolding techniques to engineer complexes with weak antiferromagnetic interactions restricted to two or fewer dimensions. Copper(II) spin ladder complexes, an interesting case of the quasi one-dimensional quantum Heisenberg antiferromagnet (1D-QHAF), can be achieved via a number of synthetic pathways. However, to design molecular magnets for detailed studies of a theoretically described regime, more robust synthetic routes are required, especially, for instance, in the reproducible synthesis of isotropic ($J_{rung} = J_{rail}$) spin-ladders.

Diazine linkages have been used to engineer chains[13,14] and layered systems[15,16] as well as ladders, including the compounds Cu(quinoxaline)X_2 and Cu(2,3-dimethylpyrazine)X_2 (X = Cl, Br).[6] In these complexes, the exchange across the rungs is ~ 50% greater than that along the rails; for example, the fitted experimental data for Cu(quinoxaline)Br_2 gave J_{rung} = -18.8 K, J_{rail} = -11.9 K (J_{rung}/J_{rail} = 1.58). Here, the rail interaction is propagated via the diazine linkage and the rung interaction via a bridging bihalide pathway. Copper(II) halide (CuX_4^{2-}) based ladders in both the strong rung (BPCB)[7,8,17] and strong rail (DIMPY)[18,19] limit have been characterized previously in terms of exchange anisotropy and Luttinger liquid models on the ladder based lattice.[9] $(5NAPH)_2CuBr_4 \cdot H_2O$ is a nearly isotropic spin ladder with J_{rung}/J_{rail} = 1.04 (J_{rung} = -10.2 K and J_{rail} = -9.8 K) where both the rung and rail bridges are two-halide pathways.[20] $(5NAPH)_2CuBr_4 \cdot H_2O$ and Cu(quinoxaline)Br_2, while somewhat isotropic, have exchange interactions strong enough that magnetization experiments to saturation, including low temperature

magnetization and field dependent neutron scattering experiments, are difficult due to the high saturation fields (> 30 T) . Thus, a weaker, isotropic, antiferromagnetic spin ladder allowing detailed field-dependent studies at lower fields still needed development.

Ladder-based lattices may be equally described as coupled chains or stacked dimers. The coupling along the chain is J_{rail} and the dimer coupling is J_{rung} (Figure 1a). The singlet-triplet gap, Δ, characteristic of all dimeric lattices is closed upon application of H_{c1}, the lower critical field, and the moment is saturated at H_{c2}.[21] Between the two critical fields, the ladder exists as a Tomonaga-Luttinger Liquid (TLL).[22] The magnetic behavior of ladders is dependent on the number of ladder rails, with even numbers giving a singlet ground state with an energy gap Δ, the size of which depends on the ratio J_{rung}/J_{rail},[3] while an odd number of rails gives a gapless doublet ground state. Coupled-ladder lattices have been investigated for their quantum critical behavior and quantum phase transitions.[23,24,25] The isotropic regime, where $J_{rail} = J_{rung}$, is a previously understudied TLL state between H_{c1} and H_{c2} and thus detailed specific heat, magnetization and NMR experiments probing the attractive or repulsive nature of the fermionic excitations (a function of K, the TLL parameter) may reveal interesting quantum effects.[26] Furthermore, thermal conductivity reaches a minimum near the isotropic point [$J_{rail} = J_{rung}$] according to perturbation theory, and thus experimental examples of this regime should allow an examination of theories.[27]

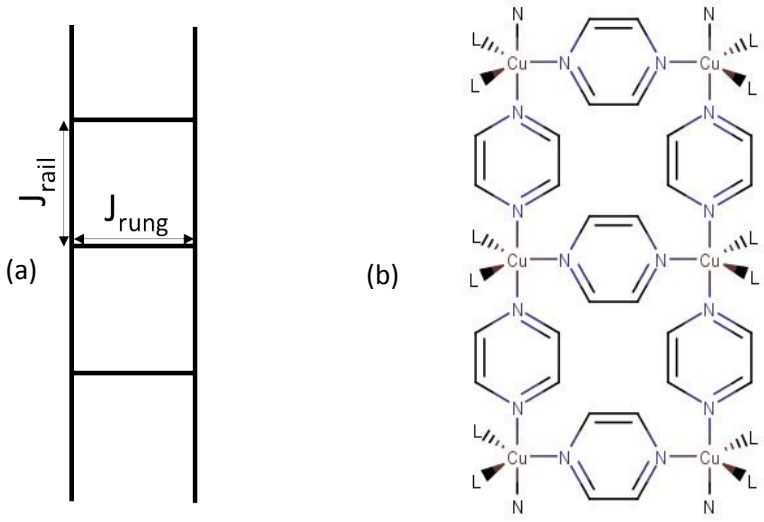

Figure 1. (a) Convention used for superexchange coupling in a ladder. (b) Line-drawing of the all-pyrazine bridged ladder scaffolding where L is a substituted capping molecule (anions are not shown).

Pyrazine-bridged systems, in particular, offer a predictable structural scaffold due to the linear nature of the ligand coordination sites (Fig. 1b), as well as a predictable exchange constant between Cu(II) ions,

usually 5-18 K, with a diverse range of systems having been demonstrated.[15,28,29,30,31] It has been suggested that the "all-pyrazine-bridged" ladder (where the pyrazine bridges lie in the Cu-equatorial plane) would approach the isotropic regime where $J_{rail} = J_{rung}$ in a predictable fashion with modest exchange, thus enabling said investigations of the field dependent behavior of the full magnetic excitation spectrum.

We recently reported the serendipitous preparation of the first all-pyrazine bridged ladder, $[Cu_2(pz)_3(4\text{-}HOpy)_4](ClO_4)_4$ [4-HOpy = 4-hydroxypyridine].[32] The compound exhibits a J_{rail}/J_{rung} ratio of 0.87, placing it among the most isotropic ladders reported, but with modest exchange strengths allowing for ready study over the full phase diagram. However, given the unexpected nature of the original synthesis, there was a question of whether a family of such materials could be prepared with variable J_{rail}/J_{rung} ratios allowing for detailed studies near the quantum critical point. We report here a convenient route for preparing isolated, nearly isotropic spin-ladders using the all-pyrazine bridge scaffold through the addition of two new all-pyrazine ladders, $[Cu(pz)_{1.5}(L)_2](ClO_4)_2$ (where L is 3-X-4-pyridone (3-X-4-HOpy) and X = Cl, Br), which are investigated structurally, magnetically and theoretically (Figure 1b). A detailed description of the X-ray crystal structure is used to inform the observed magnetization and magnetic susceptibility and to provide the basis for theoretical calculations. It becomes clear that variation of the identity of L allows tuning of the isotropic exchange strength through the pyrazine bridges by modifying the electronic character of the copper(II) ion. The Hamiltonian used in this study is shown in Equation 1, where A (B) stands for a spin-carrying unit, and negative J_{AB} represents antiferromagnetic (AFM) interactions.

$$\hat{H} = -2\sum_{(A,B)} J_{AB}\hat{S}_A \cdot \hat{S}_B \quad \text{(Equation 1)}$$

Experimental

3-Chloro-4-hydroxypyridine was purchased from Oxchem Corp. 3-Bromo-4-hydroxypyridine was purchased from Ark Pharm. Inc. Pyrazine and copper(II) perchlorate hexahydrate were purchased from Alfa Aesar. All starting materials were used as received. IR spectra were collected on a Perkin Elmer Spectrum 100 FT-IR. Combustion analyses were performed at the Marine Science Institute, University of California Santa Barbara, CA. Powder EPR spectra were collected with a Bruker EMX EPR spectrometer operating at X-Band (9.7 GHz) with a 100 kHz field modulation. Powder X-ray diffraction data were collected using a Bruker AXS-D8 Focus diffractometer.

Synthesis

$[Cu(pz)_{1.5}(3\text{-Br-4-HOpy})_2](ClO_4)_2$ [*catena*-bis(pyrazine)bis(3-bromo-4-pyridone-κ-O) (μ-pyrazine)dicopper] diperchlorate (**1**): $Cu(ClO_4)_2{\cdot}6H_2O$ (0.7723 g, 2.084 mmol) was dissolved in 3 ml H_2O. 3-Bromo-4-hydroxypyridine (0.1713 g, 0.9845 mmol) was dissolved in 18 ml methanol and was added to the $Cu(ClO_4)_2$ solution. Pyrazine (0.1770 g, 2.210 mmol), dissolved in 50/50 H_2O/methanol (4 ml), was added to this solution which was stirred for 5 minutes and then left at room temperature to slowly evaporate. After seven days, a small amount of precipitate was removed from the solution by gravity filtration. The filtrate was left to evaporate further and after several weeks green crystals of **1** were isolated by filtration, washed with water and methanol and allowed to air-dry (120 mg, 33%). IR (cm^{-1}) 3289 (broad, w), 3113 (mult, w), 1637 (med), 1571 (med), 1551 (s), 1519 (s), 1430 (med), 1389 (med), 1232 (w), 1123 (s,sh), 1097 (vs), 1062 (vs, sh), 1036 (s), 916 (w), 882 (w), 826 (med), 620 (s), 582 (w), 571 (w). CHN Found (%): C; 25.87, H; 2.42, N; 9.36. Calculated (%): C; 26.3, H; 1.93, N; 9.59.

$[Cu(pz)_{1.5}(3\text{-Cl-4-HOpy})_2](ClO_4)_2$ [*catena*-bis(pyrazine)bis(3-chloro-4-pyridone-κ-O) (μ-pyrazine)dicopper] diperchlorate (**2**)**:** $Cu(ClO_4)_2{\cdot}6H_2O$ (0.5671 g, 1.531 mmol) was dissolved in 5 ml methanol and was combined with a solution of 3-chloro-4-hydroxypyridine (0.1283 g, 1.323 mmol) in 15 ml methanol with stirring giving a green solution. Pyrazine (0.2353 g, 2.938 mmol) in 10 ml methanol was added to this solution giving a green precipitate which was filtered from the solution. The filtrate was left to evaporate slowly. Two weeks later green crystals of **2** were isolated and washed with methanol (115 mg, 36%). IR (cm^{-1}) 3283 (broad), 3113 (w, mult), 1637 (med), 1571 (med), 1551 (s), 1519 (s), 1430 (med), 1389 (w), 1232 (w), 1154 (med), 1123 (s, sh), 1097 (vs, mult), 1062 (vs, mult), 1036 (vs, sh), 882 (s), 697 (w, doublet), 620 (s), 582 (w), 571 (w, doublet). CHN Found (%): C; 29.55, H; 2.27, N; 10.62. Calculated (%):C; 29.95, H; 2.20, N; 10.91.

Magnetism

The magnetic susceptibility from 1.8 to 310 K at 1 kOe and the magnetization at 1.8 K from 0 to 50 kOe of **1** and **2** were collected on a MPMS SQUID magnetometer on powdered samples and corrected for the temperature independent paramagnetism of the Cu(II) ion and the diamagnetic contributions of the sample holder (measured independently) and the constituent atoms (estimated from Pascal's constants). No hysteresis was observed in the magnetization of **1** nor **2** (see SI, Section I, Fig. SI.1). The samples studied were confirmed to be of the same phase as the single crystal structures by comparison of the powder X-ray diffraction pattern to that calculated from the single crystal data (SI Section I, Figures SI.2 and SI.3 in the Supplementary Information). Minor differences are observed due to the difference in temperatures: RT (powder) vs. 120 K (single crystal).

X-Ray

The structures of **1** and **2** were collected at 120(2) K on a SuperNova, Dual Atlas diffractometer and processed in CryAlisPro.[33] An absorption correction from spherical harmonics using SCALE3 ABSPACK scaling algorithm was applied to the data. The structures of **1** and **2** were solved with SHELXS-97.[34] **1** and **2** were refined in SHELXL-2018[35] with all hydrogen atoms placed in geometrically calculated positions using a riding model with fixed isotropic thermal parameters. Attempts to refine the positions of the N-H protons of the substituted 4-hydroxypyridine ligands without restraints were unsuccessful. They were thus fixed in geometrically calculated positions at 0.86 Å from N11/N21 (Figures 2 and SI Section I, Figure SI.4). The pyridone molecules in **1** were modeled with 2-site disorder and final occupancies of 0.558(7)/0.442(7) (N11 ring) and 0.681(11)/0.319(11) (N21 ring). The disorder of the non-coordinated perchlorate ion in **1** proved particularly difficult to model and thus we considered the structure with the disordered perchlorate ion present in the lattice, with necessary restraints, as well as refining the structure by removing the electron density of the disordered perchlorate through the use of SQUEEZE.[36] Full details of both refinements are presented in the Supplementary Information. The non-coordinated perchlorate ion in **2** was disordered and treated with a two-site model. The final occupancies refined to 0.517(4)/0.483(4). Attempts to further define the disorder did not improve the refinement. The structures have been deposited with the CCDC as: 209943(**1-nm**)(without the solvent mask), 209944 (**1**)(using the SQUEEZE result) and 2099919 (**2**).

Theoretical Methods

The standard static first-principles bottom-up (FPBU) procedure[37] was applied to study and rationalize the magnetism of **2**. According to FPBU, first, after inspection of the crystal structure, the symmetry-unique pairs of magnetic ions that are likely to be magnetically relevant are identified (using an ion···ion distance cutoff value between spin-carrying moieties). Second, their magnetic exchange interactions, J_{AB}, are computed at UB3LYP[38] level using Gaussian09[39] (see SI Theory Sections III.1, III.2 and III.3 for further discussion on the choice of basis set and cluster model to assess J_{AB} interactions). The evaluation of J_{AB} was carried out using a 6-31+G(d) basis set,[40] which includes polarization and diffuse functions and is best suited to describe anions such as perchlorate, hydrogen bonding, Cu···O semi-coordination and other electrostatic interactions. The magnetic topology of the crystal (i.e., the network of connectivity defined by all relevant J_{AB} values) is then defined. Third, the Heisenberg Hamiltonian is applied to a model space (i.e. a subset of the magnetic topology), which is designed in such a way that, ideally, the resulting set of eigenvalues reproduces those that result from the application of the Heisenberg Hamiltonian to the full infinite crystal. Next, the resulting energies and total spin numbers are introduced into the proper statistical mechanics expressions to calculate the macroscopic properties of the system, such as the

magnetic susceptibility χ(T), heat capacity C_p(T) and magnetization M(H).[41] Finally the calculated data is compared to the experimentally measured data to make sure the FPBU procedure worked correctly.

Complementary to heat capacity $C_p(T)$, the magnetic capacity $C_s(T)$ will be evaluated to assess the importance of long-range spin correlation in **2**, since the analysis of the magnetic wavefunction enables both the study of the 3D propagation of two magnetically connected spins, i.e. short-range ordering, and magnetically non-connected spin alignment, i.e. long-range spin order/disorder.[42] Additionally, we will monitor the temperature dependence of the magnetic correlation between all spin units to draw conclusions about the ground state of the system under consideration.

Results and Discussion

Synthesis

Crystals of **1** and **2** were grown via slow evaporation from aqueous alcohol (**1**) or MeOH (**2**). The use of stoichiometric amounts of the ligands 3-chloro-4-hydroxypyridine and 3-bromo-4-hydroxypyridine was avoided because they preferentially crystallize from solution. The ligands 3-X-4-HOpy are only appreciably soluble in methanol and thus synthesis in other solvent systems was not investigated. Pyrazine can be added in excess to avoid crystallization of the linear-chain complex $[Cu(pz)(3\text{-X-4-HOpy})_2(H_2O)_2](ClO_4)_2$[43] and since the complex $[Cu(pz)_2(3\text{-X-4-HOpy})_2](ClO_4)_2$ does not form in these conditions. Reactions in aqueous solutions are also more likely to precipitate the $[Cu(pz)(3\text{-X-4-HOpy})_2(H_2O)_2](ClO_4)_2$ compounds. The product $[Cu(pz)_2](ClO_4)_2$[31] is also an issue because it is insoluble in methanol and thus a small amount of this complex precipitates from solution and oftentimes crystallizes with the desired products. The precipitation of $[Cu(pz)_2](ClO_4)_2$ can be minimized by adding pyrazine slowly. The ligand 3-X-4-HOpy can exist as either the hydroxypyridine or the pyridone tautomer; the pyridone tautomer is observed in **1** and **2**.

$$Cu(ClO_4)_2\cdot 6H_2O + 1\text{-}2\ (pz) + 0.5\text{-}1\ (3\text{-X-4-HOpy}) \xrightarrow[\text{slow evaporation}]{\text{methanol/water}} [Cu(pz)_{1.5}(3\text{-X-4-HOpy})_2](ClO_4)_2$$

Scheme 1. Synthesis of **1** (X = Br) and **2** (X = Cl).

Structures:

Parameters related to the crystal structure solution and refinement of **1** (with the solvent mask applied via SQUEEZE, which excludes one disordered perchlorate ion as seen in the parameters in Table 1) and **2** are shown in Table 1. Full comparison of compound **1**, with and without the solvent mask, may be found in

the supplementary information (Section II). Compounds **1** and **2** are isostructural, thus only the structure of **1** will be discussed in detail. Compound **1** grows as green rectangular blocks in the monoclinic space group $P2_1/c$. The asymmetric unit of **1** (see Figure SI.4) contains two 3-bromo-4-hydroxypyridine molecules, one and one-half pyrazine molecules, one copper ion, and two perchlorate ions. The two 3-Br-4-HOpy molecules are two-site disordered with the N11 ring occupancies refined to 0.56(1)/0.44(1) and the N21 ring occupancies refined to 0.68(2)/0.32(2). One of the perchlorate ions is weakly coordinated to the Cu(II) ion while the second is four-site disordered in the lattice (details may be found in the supplementary information, Section II). Cu1 is six-coordinate with nearly octahedral geometry (cis-bond angles are close to 90°, see Figure 2 and Table 2) with bonds to three pyrazine molecules, two bonds to the 3-Br-4-HOpy molecules through the pyridone oxygen atom, and one very long interaction (2.671(4) Å) to the perchlorate ion O1 atom. Thus, the coordination sphere of Cu1 is best described as a Jahn-Teller elongated, distorted 4+1+1 octahedron. One dimeric rung of the ladder in **1** is shown in Figure 2. Cu1-N bond lengths to both pyrazine[31] and 3-Br-4-HOpy[43,44] are comparable to those seen previously for related compounds (Table 2). The 3-X-4-HOpy ligands are O-coordinated and *cis*. The O14/O24-C14/C24 bonds are short (shown in Table 3) indicating significant double bond character and thus the 3-Cl-4-HOpy molecule exists as the pyridone tautomer.[45,46,47] Weak hydrogen bonding between the substituted pyridone ligands, N11-H11 and N21-H21, to the semi-coordinate and disordered perchlorate ion is observed.

Table 1. Crystallographic information for **1** (with solvent mask) and **2**. For additional details regarding **1** see SI Section II.

	1	**2**
Formula	$C_{16}H_{14}N_5O_6CuClBr_2$	$C_{16}H_{14}N_5O_{10}CuCl_4$
Molecular Weight	631.13	641.66
Crystal System	monoclinic	monoclinic
Space Group	$P2_1/c$	$P2_1/c$
a(Å)	21.4129(7)	21.3908(5)
b(Å)	6.8466(2)	6.83271(13)
c(Å)	16.6158(6)	16.4846(3)
α(°)	90	90
β(°)	99.172(3)	99.288(2)
γ(°)	90	90
V(Å)	2404.83(14)	2377.77(8)
Z	4	4
T(K)	120(2)	120(2)
ρ_{calc} (g cm^{-1})	1.73	1.792
μ(mm^{-1})	4.513	6.020

λ(Å^3)	0.71073	1.54184
Index Ranges	-26 ≤ h ≤ 25	-26 ≤ h ≤ 26
	-6 ≤ k ≤ 8	-8 ≤ k ≤ 8
	-16 ≤ l ≤ 20	-20 ≤ l ≤ 20
Indep. Reflections [I>2σ(I)]	4577	4233
Parameters	258	371
Goodness of fit	1.127	1.056
R [I>2σ(I)]	0.0469	0.0593
R_w [I>2σ(I)]	0.0927	0.1634
R (all reflections)	0.0565	0.0678
R_w (all reflections)	0.0961	0.1720

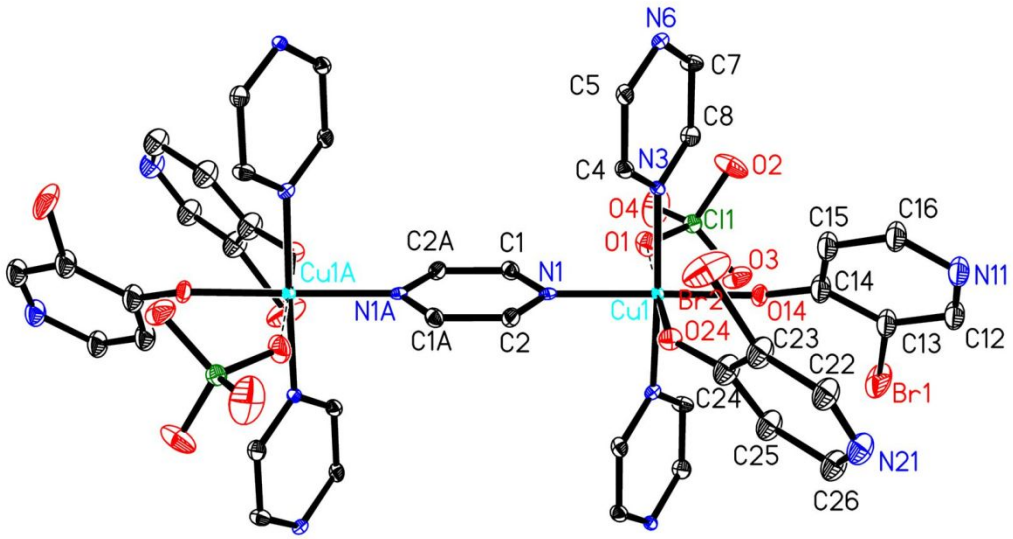

Figure 2. Thermal ellipsoid plot of a rung in **1** with the asymmetric unit labelled. Hydrogen atoms and the disordered perchlorate ion are omitted for clarity. Only the major component of the disordered pyridone rings are shown.

Table 2. Bond lengths and angles of the copper(II) coordination sphere.

	1(Å)	**2**(Å)
Cu1…O14	1.939(3)	2.203(3)
Cu1…O24	2.200(3)	1.942(2)
Cu1…N1	2.038(3)	2.037(3)
Cu1…N3	2.031(3)	2.028(3)
Cu1…N6	2.048(4)	2.040(3)
Cu1…O1	2.671(6)	2.652(4)
	1(°)	**2**(°)
O14 Cu1 O24	95.47(12)	96.34(11)

O14 Cu1 N1	171.60(13)	92.14(11)
O14 Cu1 N3	95.02(13)	91.11(10)
O14 Cu1 N6	86.50(13)	93.43(10)
O24 Cu1 N1(°)	91.96(12)	170.70(12)
O24 Cu1 N3	91.81(13)	94.46(11)
O24 Cu1 N6	93.76(13)	86.69(11)
N1 Cu1 N3	88.65(14)	89.17(11)
N1 Cu1 N6	89.11(14)	89.00(11)
N3 Cu1 N6	174.06(13)	175.16(12)

Table 3. C=O bond lengths in **1** and **2** (major contributors).

C=O	**1**	**2**
O14...C14(Å)	1.280(5)	1.253(5)
O24...C24(Å)	1.271(5)	1.268(5)

Table 4. Pertinent Cu…Cu distances in **1** and **2** and the angle between the copper(II) coordination plane (Cu1, N1, N3, N6, O14) and pyrazine rings (labelled by the bonded nitrogen atom).

	1(Å)	**2**(Å)		**1**(°)	**2**(°)
Cu…pz…Cu (J_{rail})	6.847(1)	6.8327(2)	N1	90.5	91
Cu…pz…Cu (J_{rung})	6.842(1)	6.8424(6)	N3/N6	51.0	50.9
Cu…Cu (*a*-direction)	15.560(1)	15.5362(7)			
Cu…Cu (*c*-direction)	7.872(1)	7.8233(6)			

There are two types of bridging pyrazine molecules in **1** and **2** creating a ladder structure as shown in Figure 3a. The pyrazine molecule forming the rungs lies on a crystallographic inversion center, linking the rails in **1**. The rail-type bridging pyrazine molecule links copper centers into chains in the *b* direction. Ladders are separated from each other parallel to the *a*-axis by the bulk of the ligands L (3-Cl-4-HOpy) giving a very large separation (15.6(1) Å). There is a smaller degree of separation between adjacent ladders parallel to the *c*-axis (7.87(1) Å), giving approximately a lattice of stacked ladders. The ladders, however, are offset from each other in the *c*-direction such that the semi-coordinated perchlorate ions are weakly hydrogen bonded to the pyrazine ligands from the adjacent ladder and thus there is no reasonable superexchange pathway present. The packing of **1** is shown in Figure 3b, viewed parallel to the ladder (*b*) direction. The angles that the planes of the pyrazine molecules make with the copper(II) coordination plane containing the atoms Cu1, N1, N3, N6, O14 are shown in Table 4 alongside the relevant Cu1···Cu1 distances. The non-coordinated perchlorate ion is severely disordered and full refinement details are provided in the Supplementary Information (Section II). The disordered perchlorate ion occupies a void

between ladders in the *bc* plane and causes increased separation of the ladders from one another in the *a*-direction (Figure 3b). Compound **2** is isostructural with **1** as shown in Tables 2-4. The asymmetric unit of **2** is shown in Figure SI.5. It appears the size difference between chlorine and bromine does not cause a drastically larger unit cell, most likely because the 3-substituents occupy a void in the structure. The largest percent difference in unit cell parameters is 0.8 % in the *c*-direction, while the angle β increases by 0.1 % in **2** compared to **1** despite the 5.8 % increase in van der Waals radii on going from chloride to bromide. There are no significant hydrogen bonds to the halogens.

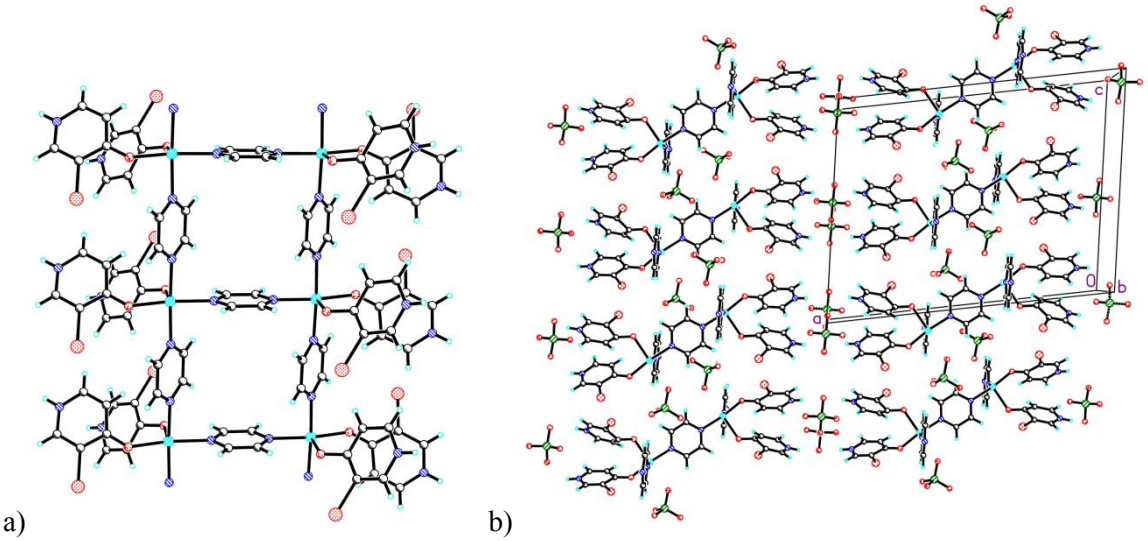

Figure 3. (a) the pyrazine bridged ladder structure of **1**, perchlorate ions and hydrogen atoms are omitted (b) packing of ladders showing separation in the *a*-direction and stacking in the *c* direction (vertical). All non-hydrogen atoms are shown as 50% thermal ellipsoids; hydrogen atoms are spheres of arbitrary size.

Magnetization

As shown in the supporting information for both compounds (SI Section I Figure SI.1), the magnetization per mol is linear up to 10 kOe, indicating the susceptibility data at 1 kOe is within the necessary regime of the magnetic field (H) going to zero. At 1.8 K **1** and **2** are still approaching a singlet ground state and thus H_{c1} is not observable; lower temperature and higher field magnetization studies are necessary to observe and quantify H_{c1} and H_{c2}. The moments at 5 T for **1** and **2** are similar and about 500 emu/mol; the moment is still increasing indicating the sample is far from saturation (~ 6000 emu/mol) as expected for an exchange coupled Cu(II) compound. The upward curvature of the plots of M(H) for **1** and **2** indicates a low-dimensional lattice dominated by quantum fluctuations, in agreement with the ladder model. The saturation fields calculated from mean-field approximation[21] are 27 T (**1**) and 28 T (**2**) using the average g-factor from susceptibility measurements (*vide infra)*.

Magnetic Susceptibility

The magnetic susceptibility of **1** reaches a maximum at 9.4 K with a value of 0.0178 emu/mol·Oe before rapidly decreasing to 0.00447 emu/mol·Oe as the temperature decreases to 1.8 K (Figure 4a). This behavior suggests the presence of a singlet ground state. With the structure and susceptibility data in mind, only an array of dimers, isolated or coupled (as in ladders or alternating chains), would be expected to describe the system. Because the structure of **1** contains pyrazine bridged superexchange pathways with the topology of isolated ladders, the strong-rail, strong-rung and isotropic ladder models were investigated toward fitting the magnetic susceptibility data. The susceptibility data of **1** is fit well by the strong-rung ladder model with J_{rung} = -6.07(2) K, J_{rail} = -5.27(2) K, Curie constant (CC) = 0.4398(3) (g_{ave} = 2.166) (see Table 5).[3,21] The strong-rail ladder model gave unphysical results for both **1** and **2**, and was not considered further. Structurally, an alternating chain model was not reasonable, and the fit to the data was poor as expected. A fit requiring $J_{rail} = J_{rung}$ gave J = -5.51(1) K with CC = 0.4407(1) emu·K/mol·Oe, paramagnetic impurity = 0.179 % and describes the susceptibility of **1** comparably to the fully refined fit as shown in Figure 4b. The small, fitted value for the percent paramagnetic impurity agrees well with the lack of a paramagnetic tail in the susceptibility of **1** (Table 5). Addition of a Curie-Weiss term, θ, to account for potential contributions from weak interactions between ladders (J') or diagonally across the ladder, did not improve the fit indicating that the ladders are well isolated thus supporting structural observations.

The magnetic susceptibility of **2** is analogous to that of **1** and was thus also analyzed using the ladder models (Figure 5). The fit parameters achieved from the strong-rung ladder model are shown in Table 5. The strong-rail ladder model similarly gave unphysical results. The fitted values for J_{rung} and J_{rail} show that **2** displays even more isotropic interactions than **1**. As with **1**, addition of a Curie-Weiss parameter did not improve the quality of fit (θ refined to zero within the error). Likewise, the susceptibility of **2** was fitted with the requirement that $J_{rail} = J_{rung}$ which gave $J_{rail} = J_{rung}$ = -5.91(2) K, CC = 0.4399(4) emu·K/mol·Oe (g_{ave} = 2.173) and a paramagnetic impurity = 0.346(14) %, a similar result as shown in Fig. 5b.

Table 5. Best least squares parameters for J_{rail}, J_{rung}, average gyromagnetic factor, and paramagnetic impurity from fits of χ(T) to the strong-rung ladder model for **1** and **2**. Estimates of the spin gap Δ from strong-rung limit and low temperature fitting.

	CC (emu·K/mol·Oe)	g_{ave}	J_{rail} (K)	J_{rung} (K)	Para (%)	J_{rail}/J_{rung}	Δ/J_{rung}	$\Delta/J_{rung}^{low\ T}$
1	0.4398(3)	2.116	-5.27(2)	-6.07(2)	0.82(2)	0.867	0.51	0.58
2	0.4427(3)	2.173	-5.80(2)	-6.12(2)	0.621(14)	0.946	0.50	0.55

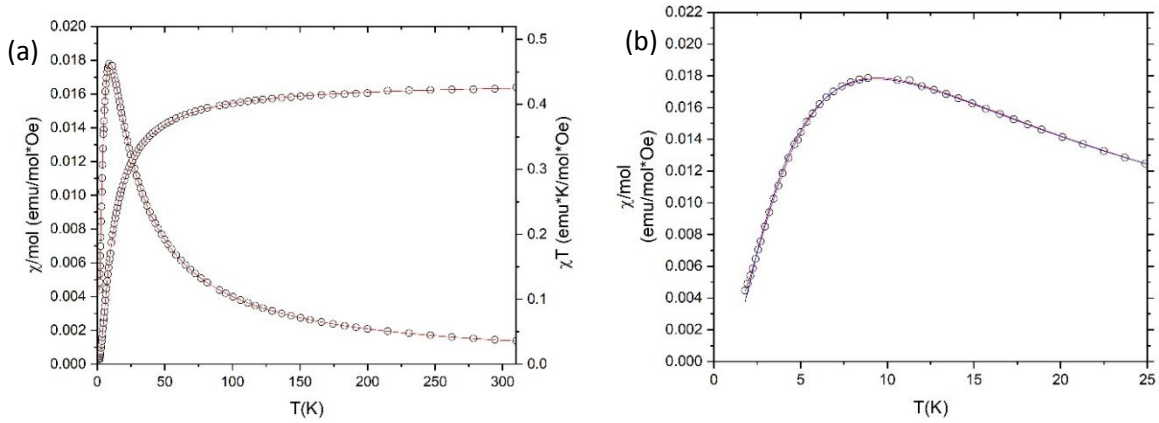

Figure 4. (a) Magnetic susceptibility of **1** plotted as χ vs. T and χT vs. T (open circles) showing the fit to the strong rung ladder model in red. (b) Magnetic susceptibility from 1.8K to 25K of **1** with the best least squares fit to the strong-rung ladder model in red with the isotropic fit shown in blue.

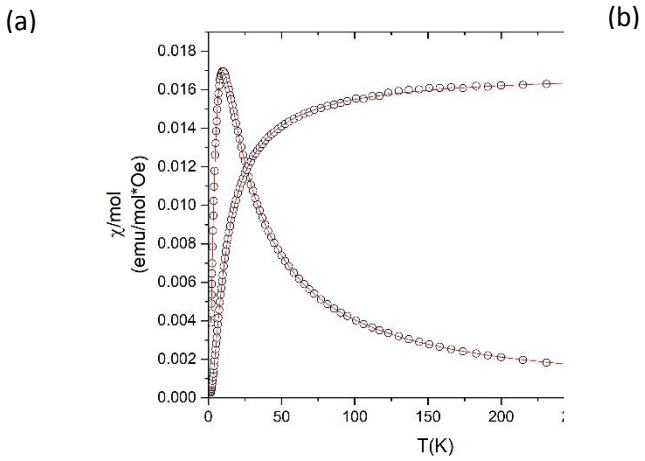

Figure 5. (a) Magnetic susceptibility of **2** plotted as χ vs. T and χT vs. T showing the fit to the strong rung ladder model in red with data shown as open circles. (b) Magnetic susceptibility from 1.8K to 25K of **2** with the best least squares fit to the strong rung ladder model in red and the isotropic fit shown in blue.

The antiferromagnetic exchange through the pyrazine linkages is typical of copper(II) complexes as the superexchange strength through pyrazine usually varies from -5 to -18 K.[16,30,31,32,43,48] The J_{rail}/J_{rung} ratio derived from the fits to the strong-rung ladder model shows that these two complexes exhibit nearly isotropic exchange (**1**: 0.867, [1.02]; **2**: 0.946, [0.978]; the fits from χT(T) are shown in brackets]. Given the structure of the complexes, being approximately 4+2 with the elongation axis perpendicular to the Cu-pyrazine coordination plane, the two types of bridging pyrazine molecules are bonded through the d_{x2-y2} orbital of the copper(II) ion much like the pyrazine bridged layers with less than four-fold symmetry

which also give nearly square or square interactions.[29,31,48] The previously best realization of an isotropic spin ladder is $(5NAPH)_2CuBr_4$ H_2O with J_{rung} = -10.2 K and J_{rail} = -9.8 K (J_{rung}/J_{rail} = 1.04).[20] Unfortunately, the magnetization does not saturate up to 30 T due to the strong exchange. It was thus necessary to find a system with weaker isotropic exchange in order to achieve saturation in an experimentally convenient field.

Not all spin-ladders consist of perfectly isolated one-dimensional ladders. Theoretical analysis of the presence of an inter-ladder coupling (J')[24] will induce 3D ordering at zero field for isotropic ladders in the case of $J'/J \geq 0.16$. One compound has been demonstrated to undergo such a zero-field transition.[12] However, the excellent agreement between the experimental susceptibility data and the 1D spin-ladder models supports ignoring the presence of a significant J' in the analysis. The all-pyrazine scaffold has afforded this regime experimentally, as evidenced by **1** and **2**. At J'/J = 0.16 a quantum critical point occurs.[12,24] However as the fits to χ(T) with the Curie-Weiss term suggest, J' is negligible and thus these compounds are not in this regime. Perhaps a smaller semi-coordinate anion such as NO_3^- would allow J' to increase and thus perhaps this interaction might be likewise tunable.

The identity of L provides only slightly different values for the exchange strength between **1** and **2** as expected since the only difference is the identity of the substituent at the 3-position of the 4-pyridone molecule. In order to develop magneto-structural correlations for the all-pyrazine bridged ladders, a large number of complexes need to be synthesized where the ligand L is varied to give either overall withdrawing or donating properties. The same process is underway with complexes of the types $[Cu(pz)(L)_2(H_2O)_2](ClO_4)_2$,[49] $[Cu(pz)(L)_4](ClO_4)_2$, and $[Cu(pz)_2(L)_2](ClO_4)_2$.

The spin gap was also estimated in this study for **1** and **2** using various methods. The energy gap Δ separating the S=0 ground state from the first S=1 excited state is approximately equal to $|0.5 \cdot 2J|$[3,4] giving $|\Delta|$ = 5.8 K (**2**), 5.6 K (**1**) based on the isotropic J values $J_{rail} = J_{rung}$ = -5.51 K (**1**) and -5.91 K (**2**). According to the expression in second order J_{rail}/J_{rung} from Ref. 50, which agrees well with numerical results in the strong rung limit,[51,52] Δ/J_{rung} = 0.51 (**1**) and 0.50 (**2**). Fits to the low-temperature region of the magnetic susceptibility with Equation 2 from Ref 52 give $|\Delta/J_{rung}|$ = 0.58 (**1**) and 0.55 (**2**) (see Table 5). These fitted values may be overestimates because of the small amount of paramagnetic impurity in the sample which should modify the slope at low temperatures.

$$\chi(J_{rung};T) \sim T^{-\frac{1}{2}} e^{-\frac{\Delta(J_{rung})}{T}} \quad \text{(Equation 2)}$$

Powder EPR

The powder EPR spectra of **1** and **2** were collected at X-Band at room temperature. The EPR spectrum of **1** is shown in Figure 6 and **2** is shown in Figure 7. The spectra of **1** and **2** appear to be axial rather than rhombic as is expected from the structure of the complexes. EasySpin[53] was used to fit the spectra assuming one spin; the fit parameters are presented in Table 6. The g-tensor was allowed to refine with rhombic freedom despite the axial appearance of the spectra, and the fitted g-values agree with previous Cu(pz) compounds.[15,43,54] The linewidth was described using the parameters LWG and LWL which indicate the contribution of Gaussian and Lorentzian shapes to the line according to an approximate linear combination. G-strain, or inhomogeneous Gaussian broadening of the line was necessary to fit the data around g_z since G-strain is proportional to g.

The fit parameters for **1** and **2** are similar as expected from the structure of the complexes. The fit to **1** gives a slightly rhombic g-tensor since $g_x \neq g_y \neq g_z$ while that of **2** refines to an axial g-tensor with $g_x = g_y \neq g_z$. The calculated value for g_{ave} (2.144 (**1**), 2.143 (**2**)) from EPR results agrees within 1.5% of that garnered from susceptibility measurements. The nearly axial spectrum is consistent with an isotropic exchange through the pyrazine rungs and rails (the Jahn-Teller axis, the z-axis, is perpendicular to that plane), which interact with the x^2-y^2 orbital in a nearly identical fashion as suggested by bond lengths and angles (Table 2). Furthermore, in line with the fits to χ(T), **2** behaves slightly more axial (isotropic) than **1**. The linewidth of both **1** and **2** is somewhat large ($\approx$ 30 Gauss) compared to similar pyrazine bridged complexes.[15,43,55,56] According to the parameters LWG and LWL, the lineshape is primarily Lorentzian as expected of an exchange coupled system.[57] The amounts of g-strain indicated from the fits are somewhat large compared to similar pyrazine bridged complexes.[43]

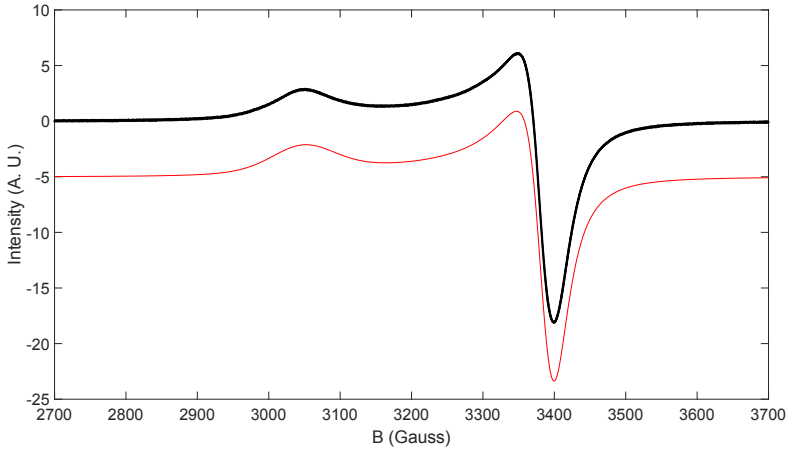

Figure 6. Powder EPR spectrum of **1** at room temperature and X-Band. Data is shown in black while the fit to the data is shown in red.

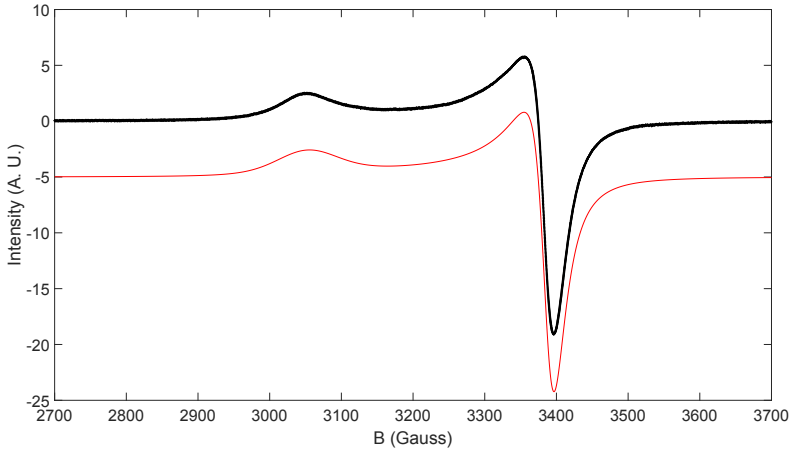

Figure 7. Powder EPR spectrum of **2** at room temperature and X-Band. Data is shown in black while the fit to the data is shown in red.

Table 6. Parameters from fits to the powder EPR spectra of **1** and **2** performed in EasySpin.

	1	2
g_x	2.0604	2.0665
g_y	2.0728	2.0665
g_z	2.2981	2.2951
LWG	0.0039	0.0946
LWL	3.2301	2.8239
gstrain	0.06	0.0575
rmsd	0.0056	0.0035

Theoretical analysis:

The lower degree of disorder in the structure indicated that **2** was the better choice for a theoretical study. Analysis of the crystal packing of **2** in terms of Cu···Cu distances shows that the pairs of spin carriers that might be magnetically important first define a spin ladder along the *b*-crystallographic direction (see Figures 3 and 8a). Note the distances giving rise to rungs and rails are uniform (6.84 Å in red and 6.83 Å in black, respectively, in Figure 8a), which means that **2** might be a nearly isotropic spin ladder. Further analysis shows that these spin ladders might be then magnetically connected along the *c*-axis (see Cu···Cu connected at ~7.8Å and ~8.9Å in Figure 8b, where spin ladders running along *b*-axis are enclosed in blue). No further magnetic coupling is foreseen along the *a*-direction because the Cu···Cu distance between spin carriers is too large (>15 Å).

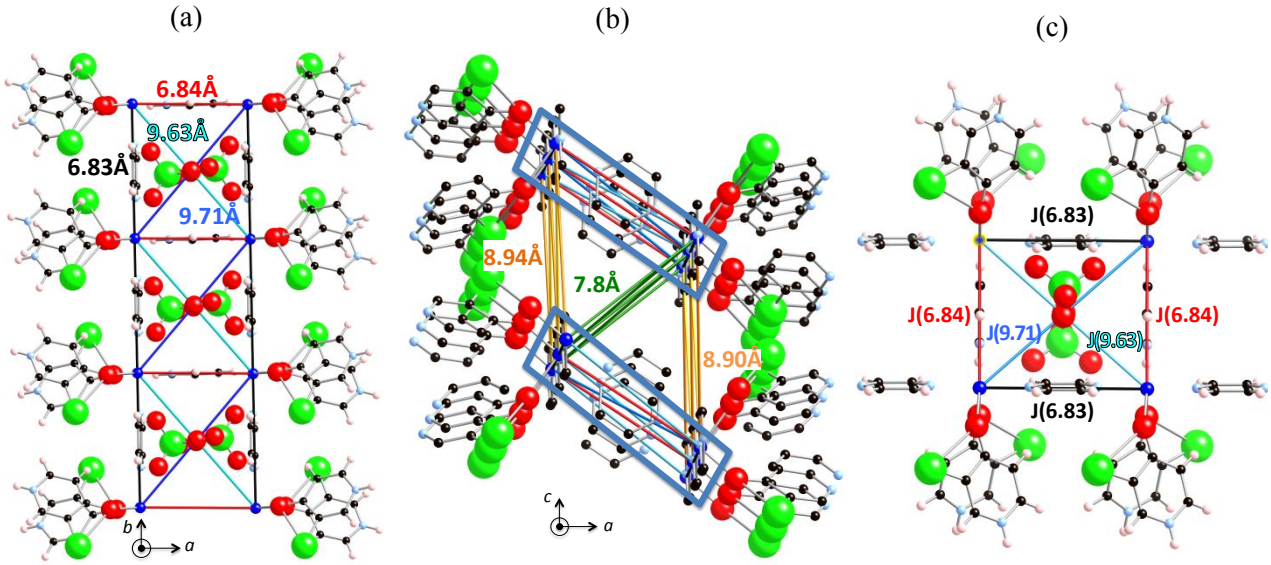

Figure 8. Crystal packing of **2** showing which radical pairs have been chosen in terms of Cu···Cu distances (a) within a spin ladder (along *b*-axis), and (b) between spin ladders (along *c*-axis). Note that the view in (b) has been chosen according to Figure 3b to enable an easier comparison. (c) Tetramer $[Cu4A4]^{4+}$ cluster model used to compute the J_{AB} magnetic interaction between pairs of Cu-moieties. Color code: J_{AB} mediated by pyrazines: J(6.83) in black and J(6.84) in red; and through-space J_{AB} interactions: J(9.63) in cyan, and J(9.71) in blue. Note that # in J(#) stands for the distance between Cu ions in angstroms (i.e. J(6.83) = J_{AB} for 6.83 Å Cu···Cu separation). Note that significant distances as dashed lines are also shown between main Cu···pz···Cu scaffolding and ligands (H_2O and perchlorates) (in (c) right).

In order to evaluate the J_{AB} magnetic coupling between Cu-spin moieties, different tetramer models (see Figure 8c for an example) were selected to calculate J_{AB} between intra-ladder spin carriers at 6.833Å (black, along the *b*-axis) connected by either shortest interdimer contacts, 6.842 Å (red in Figure 8a), or by next shortest interdimer contacts, 7.823 Å (green in Figure 8b). Let us remark that the choice of tetramer models was made paying special attention to which weak interactions have to be included in order to describe adequately the environment of each spin carrying center (see SI Theory Section III.3 for full details on the cluster models used to calculate all J_{AB} magnetically important couplings). Therefore, the evaluation of the J_{AB} magnetic coupling between pairs of Cu-moieties was suited to include the effect of anions such as perchlorates, hydrogen bonding, Cu···O semi-coordination and other electrostatic interactions. Additionally, it was also assessed whether pairs of spin carriers connected along the *c*-axis at 8.902 and 8.942 Å (i.e. inter-ladder couplings) were magnetically important. Notice that magnetic interactions between Cu-moieties at 6.833 and 6.842 Å are mediated by a pyrazine ligand, while all others are through-space magnetic interactions.

Our results show that only interactions between Cu-moieties connected by a pyrazine ligand are magnetically significant (see J(6.83) and J(6.84) in Table 7). This result is consistent with the fact that the Cu-moieties are significantly further apart in all other through-space Cu···Cu magnetic couplings between spin carriers. Computed data provide a value of both J_{AB} magnetic couplings of *ca.* −2.50 cm^{-1} (-3.6 K) if no perchlorate counterions are taken into account, irrespective of the tetramer model used to calculate the magnetic coupling between Cu-spin carriers (see Cu4 model in Table 7). This value becomes more antiferromagnetic (AFM) reaching *ca.* −4.00 cm^{-1} (-5.8 K) when the perchlorates are considered (see Cu4A4 model in Table 7). Let us stress here that the perchlorate ClO_4^- counterions simply affect the Madelung field and, thus, their main role is purely electrostatic. It has been found that slightly larger J_{AB} values are computed if the two-dimensional (2D) Cu···pz···Cu scaffold is only partially described (see full discussion in SI Section III.3). It can thus be concluded that it is crucial to include both the all-pyrazine bridge Cu···pz···Cu scaffold geometry of both meaningful J(6.83) and J(6.84) magnetic interactions, and the appropriate semi-coordinate counterions, which are inferred to be four anions, to calculate the J_{AB} magnetic coupling between Cu-moieties in compound **2** (see Cu4A4 model with J(6.83,rail) = -4.04 cm^{-1} and J(6.84,rung) = -3.89 cm^{-1} in Table 7; see SI Theory Section III.3 for further discussion).

According to the above results, the magnetic topology consists of isolated magnetic spin-ladders with almost isotropic J(6.84) AFM rungs (in red) and J(6.83) AFM rails (in black) (see Figure 9), which is again consistent with the experimental data. Therefore, a single magnetic spin-ladder model will be used to reproduce the available experimental magnetic susceptibility and magnetization data (Note that the experimental g_{avg} value extracted from EPR experiments was employed in all simulations). In addition, we will estimate whether long-range magnetic order is to be observed and the value of the temperature below which it would be realized.

Table 7. UB3LYP/6 -31+G(d) computed J_{AB} values (in cm^{-1}, values in parentheses are in K). In J(#), # stands for the distance between Cu ions in Angstroms (i.e. J(7.82) stands for J_{AB} with a Cu···Cu separation of 7.82 Å). Note that "J(9)" stands for the average between J(9.63) and J(9.71) values.

model	**J(6.83)**	**J(6.84)**	**J(7.82)**	**J(8.90)**	**J(8.94)**	**"J(9)"**
Cu4	-2.41 (-3.42)	-2.84 (-4.56)	<|0.05|	<|0.05|	<|0.05|	<|0.05|
Cu4A4	-4.04 (-5.77)	-3.89 (-5.56)	<|0.05|	-0.06	<|0.05|	<|0.05|

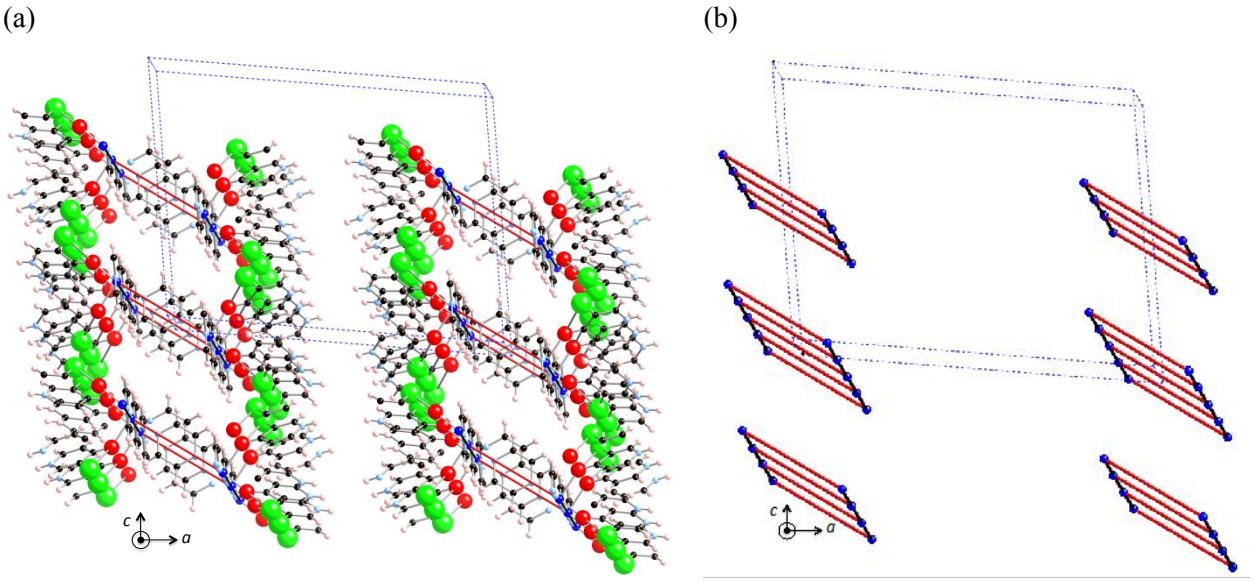

Figure 9. Magnetic topology of **2** consists of isolated AFM spin ladders, which run along the *b*-axis direction. Ladders are: (a) viewed within the Cu-pyrazine skeleton, and (b) schematically represented by replacing the entire Cu-moiety by a single Cu atom.

The experimental magnetic susceptibility data is nicely reproduced by our calculated data (see Figure 10a and SI Theory Section III.4 Figure SIII.4.1). The calculated magnetic susceptibility shows a maximum value of 0.0180 emu/mol·Oe at 9.5K, which compares extremely well with the measured 0.0173 emu/mol·Oe value at 9.4K. The calculated magnetization to 5 T at 1.8K is also in agreement with the experimental available data at 1.8K (see Figure 10b). Our experimental data also show an upward curvature of the plot of M(H) which indicates a low-dimensional lattice dominated by quantum fluctuations (see SI Section I Figure SI.1), in agreement with the ladder magnetic topology. At 1.8 K, **2** is still approaching a singlet ground state and, thus, the critical field H_{c1} is not observable; lower temperature and higher field magnetization studies are necessary to experimentally observe and quantify H_{c1} and H_{c2}. Our simulations indicate that saturation should be reached at $H_{c2} \sim 24$ T (see SI Theory Section III.4 Figure SIII.4.2). This result is in line with the estimates from both mean-field approximation (24T) and using the average g-factor from susceptibility measurements (*vide infra*) (28T).[21] As for H_{c1}, our simulations below 1.8K give an estimate of *ca*. 4.3T and indeed suggest a quantum dominated magnetic spectrum (see SI Theory Section III.4 Figure SIII.4.2). However, to be certain, it would be very useful to perform these simulations using crystallographic data characterized at temperatures *ca*. 1.8K, instead of using X-ray data characterized at 120K.[58] Further experimental measurements are thus required to corroborate our computational estimates.

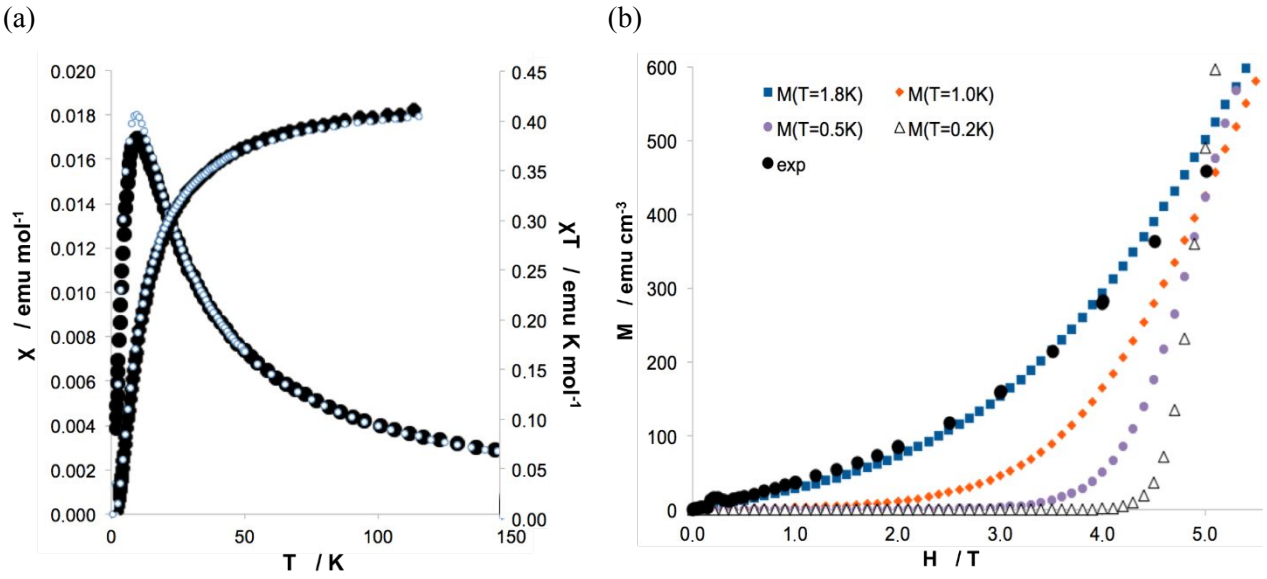

Figure 10 - Comparison of experimental and theoretical magnetic data for **2**. (a) Magnetic susceptibility as a function of temperature, where full and empty symbols represent experimental and calculated data, respectively. (b) Magnetization as a function of the magnetic field, experimental (●) and calculated at 1.8K (■), 1.0K (◆), 0.5K (●), and 0.2K (△).

Experimentally, it has long been known that temperature-dependent heat capacity studies, $C_p(T)$, at zero-field exhibit a given critical temperature at which there is either a λ-anomaly or a broad peak. The λ-anomaly would allegedly be an indication of a crossover from 2D to 3D magnetic ordering and could be attributed to long-range spin ordering. On the contrary, a broad peak would allegedly be due to short-range spin correlations. In our simulations, we work with a subset of the infinite crystal. Therefore, from our $C_p(T)$ data it would be hard to distinguish whether the main contribution to the heat capacity comes from long- or short-range spin correlations. Recently, we have put forward the magnetic capacity $C_s(T)$,[42] as a new descriptor of the magnetic topology, since it is a measure of the thermal variation of the spin multiplicity of the system and reflects the importance of magnetically non-connected spin alignment and how the dominant effect of long-range spin correlation governs the magnetic behavior of molecule-based crystals (as well as metal-coordinated molecular magnetic materials). In the same study it was also concluded that $C_p(T)$ measures the energy variation due to the 3D propagation of the interaction of two magnetically connected spins, that is, to short-range ordering. Therefore, analyzing the behavior of the critical temperature T_C of both magnetic $C_s(T)$ and heat $C_p(T)$ capacities provides information on the importance of long-range spin correlation.

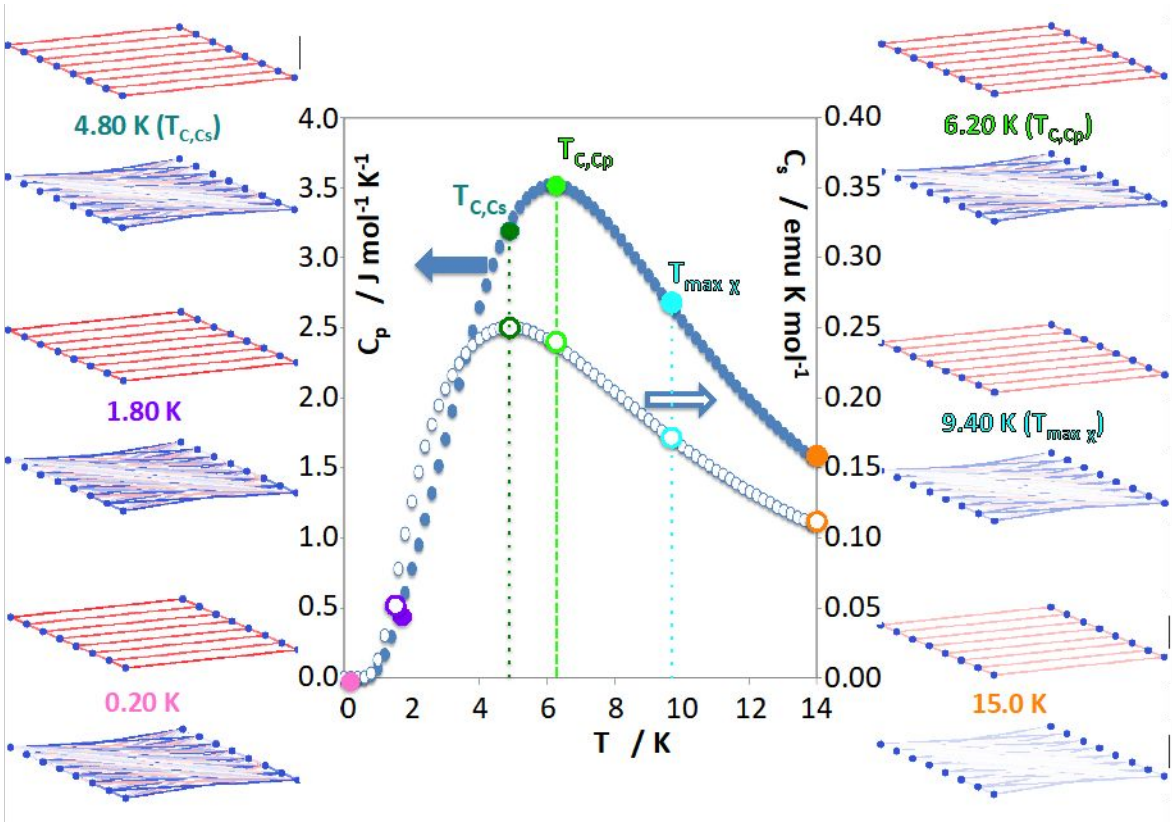

Figure 11. Heat capacity $C_p(T)$ (solid symbol, ●) and magnetic capacity $C_s(T)$ (empty symbol, ○) as a function of temperature. See inset for temperature dependence of the magnetic correlation between all spin units at 0.2 K, 1.8 K (lowest temperature of magnetization measures), 4.8 K ($T_{C,Cs}$), 6.2 K ($T_{C,Cp}$), 9.4 K ($T_{max,\chi}$) and 15 K. Upper / lower plot represents short- / long-range spin correlation between magnetic units. Note that spins coupled are represented in red, and spins arranged parallel in blue. Note also that the thickness of the lines connecting radicals is proportional to the strength of the correlation between spins.

For **2**, we discover that T_C calculated from $C_p(T)$ is 6.2K and from $C_s(T)$ is 4.8K (see Figure 11 and SI Theory Section III.4 Figure SIII.4.3). We know that a large ratio between the two critical temperatures is synonymous with a magnetic topology of high dimensionality, and with importance of long-range spin ordering. The ($T_{C,Cs}$ / $T_{C,Cp}$) ratio is 77 %, which is indicative that a 2D to 3D crossover might be feasible at low temperatures. This is, in fact, corroborated by the analysis of the magnetic wavefunction at different temperatures (see inset in Figure 11 and also SI Theory Section III.4 Figure SIII.4.4), which shows a large contribution of both short- and long-range spin correlation as already appraised up to 4.8K (i.e. $T_{C,Cs}$). Note that short-range spin ordering is purely AFM (i.e. antiparallel spin alignment, see red lines in Figure 11), while long-range is mostly FM (i.e. parallel spin alignment, see blue lines in Figure 11). From 4.8K to 6.2K (i.e. $T_{C,Cp}$), the contribution from long-range ordering becomes smaller. In fact, the non-appearance of connections between spin-carrying moieties means that there is a non-ordered spin alignment (colorless lines in Figure 11). At 9.4K ($T_{max,\chi}$), long-range order is almost lost, and at 15K it

can be discarded, whereas short-range becomes less important. It is clear that long-range spin correlation is lost at lower temperature than short-range correlation, in agreement with previous studies.[42,58]

Analysis of the Boltzmann population corroborates that the ground state is a singlet and there are accessible triplet states (see Table 8 and SI Theory Section III.4). In fact, at $T_{C,Cs}$ = 4.8 K triplet states are half of the total population within the lowest 10 magnetic states. Let us comment that, below 4.0 K, these 10 states carry up to 90% of the total spin population. At this point, one can calculate the spin gap (Δ_{gap}) as the energy difference between the singlet ground state and the first triplet state, which is obtained by solving the Heisenberg secular equation in the space defined by the minimal 2D spin ladder magnetic model. The Δ_{gap} value obtained is 4.9 cm^{-1}, i.e. 7.1K, which is in agreement with the experimental singlet and triplet spin-gap values estimated to be 5.8K. Note that Δ_{gap} extracted from the eigenvalues resulting from full diagonalization of the corresponding Heisenberg Hamiltonian results in a 4.9 T critical field ($H_{c1} = \Delta_{gap}/g\mu_B$), which indirectly supports our estimated value of 4.3 T for H_{c1}.

Table 8. Percentage of ground state, first excited state, and 2 to 9 excited states at 0.2 K, 1.8 K, 4.8 K, 6.2 K, 9.4 K and 15 K of **2**. Note that temperatures have been chosen in agreement with Figure 13. GS and ES stand for Ground and Excited States, respectively. GS, and ES6-ES7 are singlets (S=0), ES1-ES4 and ES9-ES10 are triplets (S=1) and ES5 is a quintet (S=2).

T / K	% GS	% ES1	% ES i - j (see below for States)	% 10 States	% S=1 over 10 States (GS + 9 ES)
15.0	0.37		3.41 [c]	3.78	69.4
9.4	2.80		14.93 [c]	17.74	67.6
6.2	14.57	13.95	24.42 [b]	52.94	61.6
4.8	30.95	21.26	25.71 [b]	77.91	53.4
1.8	93.64	5.51	0.79 [a]	99.94	6.3
0.2	100.0	-	-	100.0	-

[a] Percentage considering ES2-ES4; [b] Percentage considering ES2-ES9; [c] Percentage considering ES1-ES9.

Conclusion:

In conclusion, a new pyrazine bridged ladder scaffold is introduced with the formula $[Cu(pz)_{1.5}(L)_2](ClO_4)_2$. The susceptibility as a function of temperature was successfully analyzed using the strong rung-ladder model for both **1** and **2**; only a small effect on the magnitude of *J* is observed as a function of L. The superexchange strength J_{rail}/J_{rung} is nearly isotropic in this pair of isostructural complexes where L is 3-X-4-HOpy with X = Cl or Br. The potential ambiguity of a strong-rung/strong-rail evaluation of the experimental results, especially in a system so close to the isotropic point, was eliminated by theoretical analysis. Employing the computational evaluation of magnetic J_{AB} couplings

between Cu-moieties of **2** independently verifies the experimentally posited magnetic topology in agreement with isolated, nearly isotropic spin-ladders (J_{rail} = −4.04 cm^{-1} (−5.77 K) and J_{rung} = −3.89 cm^{-1} (−5.56 K) using $\hat{H} = -2\sum J_{AB}\hat{S}_A \cdot \hat{S}_B$ Hamiltonian).

Theoretical simulations of **2** are in excellent agreement with experimental χ magnetic susceptibility and magnetization down to 1.8 K. In fact, calculated magnetization data at very low temperatures (< 1.8 K), hints at the presence of quantum effects, as already indicated by measured magnetization to 5T. Additionally, calculated lower and saturation (ca. 4.3 and 24 T, respectively) critical fields for **2** are consistent with experimental estimates, although lower temperature and higher field magnetization studies are necessary to experimentally observe and quantify these two critical fields.

Further, the assessment of the short- and long-range spin ordering of **2** by evaluation of the magnetic wavefunction indicates that a 2D-to-3D crossover might be feasible at low temperatures. In fact, analysis of the Boltzmann population corroborates that there are accessible high spin multiplicity states (e.g. triplet) above the singlet ground state enabling the aforementioned 2D-to-3D crossover, and provides a value for the spin gap of 4.9 cm^{-1}, which is in turn in agreement with the experimental singlet - triplet spin gap estimated to be 5.8 K.

Preparation of additional members of this family of isostructural all-pyrazine bridged ladders is in process along with the associated studies of magneto-structural correlations. Thus, by varying the identity of L we can observe effects on the isotropic superexchange strength J. High-field, low-temperature magnetization studies up to saturation will be performed towards exploring the isotropic regime of spin ladders.

Acknowledgements

We are grateful for funds from PCI Synthesis, Inc. (now SEQENS) toward the purchase of the D8 Focus diffractometer, from the National Science Foundation (IMR-0314773) for purchase of the MPMS SQUID magnetometer, and from the Kresge Foundation for both instruments. MD acknowledges financial support from MINECO (CTQ2017-87773-P/AEI/FEDER, UE and PID2020-115165GB-I00), Spanish Structures Excellence María de Maeztu program (MDM-2017-0767), and Catalan DURSI (2017SGR348).

Disclosure statement

There are no conflicts of interest as reported by the authors.

References:

1. E. Dagotto, T.M. Rice, *Science* 1996**, 271**, 618.

2. Y. Wang, *Phys. Rev. B.* 1999, **60**, 9236.

3. D.C. Johnston, M. Troyer, S. Miyahara, D. Lidsky, K. Ueda, M. Azuma, Z. Hiroi, M. Takano, M. Isobe, Y. Ueda, M.A. Korotin, V.I. Anisimov, A.V. Mahajan, L.L. Miller, *arXiv:cond-mat/0001147v1 [cond-mat.str-el] 11 Jan 2000*.

4. I.L. Danilovich, E.V. Karpova, I.V. Morozov, A.V. Ushakov, S.V. Streltsov, A.A. Shakin, O.S. Volkova, E.A. Zvereva, A.N. Vasiliev, *Chemphyschem* 2017, **18**, 2482.

5. S.M. Bovill, R.J Dixey, P.J. Saines, *CrystEngComm* 2017, **19**. 1831.

6. J. Jornet-Somoza, N. Codina-Castillo, M. Deumal, F. Mota, J.J. Novoa, R.T. Butcher, M.M. Turnbull, B. Keith, C.P. Landee, J.L. Wikaira, J. L., *Inorg Chem* 2012, **51**, 6315.

7. A.J. Gale, C.P. Landee, M.M. Turnbull, J.L. Wikaira, *Polyhedron* 2013**, 52**, 986.

8. M. Klanjsek, H. Mayaffre, C. Berthier, M. Horvatic, B. Chiari, O. Piovesana, P. Bouillot, C. Kollath, E. Orignac, R. Citro, T. Giamarchi, *Phys Rev Lett* 2008, **101**, 137207.

9. K. Ninios, T. Hong, T. Manabe, C. Hotta, S.N. Herringer, M.M. Turnbull, C.P. Landee, Y. Takano, H.B. Chan, *Phys Rev Lett* 2012**, 108**, 097201.

10. H.S. Sousa, M.S.S. Pereira, I.N. de Oliveira, J. Strecka, M.L. Lyra, *Phys. Rev. E* 2018, **97**, 052115.

11. M. Ozerov, M. Maksymenko, J. Wosnitza, A. Honecker, C.P. Landee, M.M. Turnbull, S.C. Furuya, T. Giamarchi, S.A. Zvyagin, *Phys. Rev. B* 2015, **92**, 241113.

12. T. Hong, K.P. Schmidt, K. Coester, F.F. Awwadi, M.M. Turnbull, Y. Qiu, J.A. Rodriguez-Rivera, M. Zhu, X. Ke, C.P. Aoyama, Y. Takano, H. Cao, W. Tian, J. Ma, R. Custelcean, H.D. Zhou, M. Matsuda, *Phys. Rev. B* 2014, **89**, 174432.

13. E. Kwiatkowski, G. Romanowski, W. Nowicki, K. Suwińska, *Polyhedron* 2001, **20**, 1097.

14. J.F. Villa, W.E. Hatfield, *J. Am. Chem. Soc.* 1971, **93**, 4081.

15. M. Kubus, A. Lanza, R. Scatena, L.H.R. Dos Santos, B. Wehinger, N. Casati, C. Fiolka, L. Keller, P. Macchi, C. Ruegg, K.W. Kramer, *Inorg Chem* 2018, **57**, 4934.

16. J. Darriet, M.S. Haddad, E.N. Duesler, D.N. Hendrickson, *Inorg. Chem.* 1979, **18**, 2679.

17. E. Čižmár, M. Ozerov, J. Wosnitza, B. Thielemann, K.W. Krämer, C. Rüegg, O Piovesana, M. Klanjšek, M. Horvatić, C. Berthier, S.A. Zvyagin, *Phys. Rev. B* 2010, **82**, 054431.

18. F.F. Awwadi, R.D. Willett, B. Twamley, R. Schneider, C.P. Landee, C.P. *Inorg. Chem.* 2008, **47,** 9327.

19. Y.V. Krasnikova, V.N. Glazkov, M.A. Fayzullin, D. Schmidiger, K.Y. Povarov, S. Galeski, A. Zheludev, *J. Physics: Conf. Ser.* 2018, **969,** 012113.

20. M. Deumal, G. Giorgi, M.A. Robb, M.M. Turnbull, C.P. Landee, J.J. Novoa, *Euro. J. Inorg. Chem.* 2005, 4697.

21. C.P. Landee, M.M. Turnbull, *J. Coord. Chem.* 2014, **67**, 375.

22. a) J. M. Luttinger *J. Mathem. Phys.*, 1963, **4**, 1154. b) T. Giamarchi, *Quantum physics in one dimension*, Oxford University Press, 2004.

23. A.S. Gibbs, A. Yamamoto, A.N. Yaresko, K.S. Knight, H. Yasuoka, M. Majumder, M. Baenitz, P.J. Saines, J.R. Hester, D. Hashizume, A. Kondo, K. Kindo, H. Takagi, *Phys. Rev. B* 2017, **95**, 104428.

24. T. Giamarchi, A.M. Tsvlik, *Phys. Rev. B.* 1999, **59,** 11398.

25. B. Normand, B.; Rice, T.M. *Phys. Rev. B.* 1997, **56**, 8760.

26. M. Jeong, D. Schmidiger, H. Mayaffre, M. Klanjsek, C. Berthier, W. Knafo, G. Ballon, B. Vignolle, S. Kramer, A. Zheludev, M. Horvatic, M., *Phys. Rev. Lett.* 2016, **117**, 106402.

27. R. Steinigeweg, J. Herbrych, X. Zotos, W. Brenig, *Phys. Rev. Lett.* 2016, **116**, 017202.

28. P.A. Goddard, J.L. Manson, J. Singleton, I. Franke, T. Lancaster, A.J. Steele, S.J. Blundell, C. Baines, F.L. Pratt, R.D. McDonald, O.E. Ayala-Valenzuela, J.F. Corbey, H.I. Southerland, P. Sengupta, J.A. Schlueter, *Phys. Rev. Lett.* 2012, **108**, 077208.

29. P.A Goddard, J. Singleton, I. Franke, J.S. Möller, T. Lancaster, A.J. Steele, C.V. Topping, S.J. Blundell, F.L. Pratt, C. Baines, J. Bendix, R.D. McDonald, J. Brambleby, M.R. Lees, S.H. Lapidus, P.W. Stephens, B. Twamley, M.M. Conner, K. Funk, J.F. Corbey, H.E. Tran, J.A. Schlueter, J.L. Manson, *Phys. Rev. B* 2016, **93***,* 094430.

30. H.W. Richardson, W.E. Hatfield, *J. Am. Chem. Soc.* 1976, **98**, 835.

31. F.M. Woodward, Gibson, G.B. Jameson, C.P. Landee, M.M. Turnbull, R.D. Willett, *Inorg. Chem.* 2007, **46**, 4256.

32. S.A. Zvyagin, A.N. Ponomaryov, E. Schulze, M. Ozerov, Y. Skourski, T. Reimann, L.I. Zviagina, L. Bhaskaran, E.L. Green, J. Wosnitza, I. Sheikin, C. Kollath, P. Bouillot, T. Giamarchi, J.L. Wikaira, M.M. Turnbull, C.P. Landee, *Phys. Rev. B*, 2021, **103,** 205131.

33. *CrysAlisPro*, 1.171.38.43; Rigaku Oxford Diffraction Ltd.: 2015.

34. G.M. Sheldrick, *Acta Crystallogr A* 2008, **64**, 112.

35. G.M. Sheldrick, *Acta Crystallogr C* 2015, **71**, 3.

36. A.L. Spek, *Acta Crystallogr.. C* 2015, **71**, 9.

37. M. Deumal, M.J. Bearpark, J.J. Novoa, M.A. Robb, *J. Phys. Chem A* 2002, **106**, 1299.

38. a) A.D. Becke, *Phys. Rev. A* 1988, **38**, 3098. b) A.D. Becke, *J. Chem. Phys*. 1993, **98,** 5648. (c) C. Lee, W. Yang, R.G Parr, *Phys. Rev. B* 1988, **37**, 785.

39. Gaussian 09, Revision D.01, M.J. Frisch, G.W. Trucks, H.B. Schlegel, G.E. Scuseria, M.A. Robb, J.R. Cheeseman, G. Scalmani, V. Barone, B. Mennucci, G.A. Petersson, H. Nakatsuji, M. Caricato, X. Li, H.P. Hratchian, A.F. Izmaylov, J. Bloino, G. Zheng, J.L. Sonnenberg, M. Hada, M. Ehara, K. Toyota, R. Fukuda, J. Hasegawa, M. Ishida, T. Nakajima, Y. Honda, O. Kitao, H. Nakai, T. Vreven, J.A. Montgomery Jr, J.E. Peralta, F. Ogliaro, M.J. Bearpark, J.J. Heyd, E. Brothers, K.N. Kudin, V.N. Staroverov, R. Kobayashi, J. Normand, K. Raghavachari, A. Rendell, J.C. Burant, S.S. Iyengar, J. Tomasi, M. Cossi, N. Rega, J.M. Millam, M. Klene, J.E. Knox, J.B. Cross, V. Bakken, C. Adamo, J. Jaramillo, R. Gomperts, R.E. Stratmann, O. Yazyev, A.J. Austin, R. Cammi, C. Pomelli, J.W. Ochterski, R.L. Martin, K. Morokuma, V.G. Zakrzewski, G.A. Voth, P. Salvador, J.J. Dannenberg, S. Dapprich, A.D. Daniels, O. Farkas, J.B. Foresman, J.V. Ortiz, J. Cioslowski, D.J. Fox, Gaussian, Inc., Wallingford CT, 2016.

40. (a) P.C. Hariharan, J.A. Pople, *Theor. Chim. Acta* 1973, **28**, 213; (b) M.M. Francl, W.J. Petro, W.J. Hehre, J.S. Binkley, M.S. Gordon, D.J. DeFrees, J.A. Pople, J.A. *J. Chem. Phys*. 1982, **77**, 365.

41. (a) R.L. Carlin, *Magnetochemistry*; Springer-Verlag Berlin Heidelberg, 1986. (b) O. Kahn, *Molecular Magnetism*; VCH Publishers: New York, 1993. (c) R. Boca, *Theoretical Foundations of Molecular Magnetism. Current Methods in Inorganic Chemistry;* Elsevier Science: Amsterdam, 1999; Vol. 1.

42. J. Jornet-Somoza, M. Deumal, J. Borge, M.A. Robb, *J. Phys. Chem. A*, 2018, **122**, 2168

43. J.C. Monroe, C.P. Landee, M.M. Turnbull, J.L. Wikaira, *J. Coord. Chem*. 2020, 43**73**, 2645.

44. J.-X Yuan, M.-L. Hu, Y.-Q. Cheng, L.-C. Chen, S.W. Ng, *Acta Cryst. C* 2002, **C58**, m270.

45. J.R. Schrieffer, X.G. Wen, S.C. Zhang, *Phys. Rev. B* 1989**, 39**, 11663.

46. S. Argibay-Otero, R. Carballo, E.M. Vazquez-Lopez, *Acta Cryst. E* 2017, **73**, 1551.

47. D.M. Nguyen, V. Desikan, J.A. Golen, D.R Manke, *Acta Cryst. E* 2015, **71**, o533.

48. J.L. Manson, S.H. Lapidus, P.W Stephens, P.K. Peterson, K.E Carreiro, H.I. Southerland, T. Lancaster, S.J. Blundell, A.J. Steele, P.A. Goddard, F.L. Pratt, J. Singleton, Y. Kohama, R.D. McDonald, R.E. Del Sesto, N.A. Smith, J. Bendix, S.A. Zvyagin, J. Kang, C. Lee, M.H. Whangbo, V.S. Zapf, A. Plonczak, *Inorg. Chem.* 2011, **50**, 5990.

49. E. Kirkman-Davis, F.E. Witkos, V. Selmani, J.C. Monroe, C.P. Landee, M.M. Turnbull, L.N. Dawe, M. Polson, J.L. Wikaira, *Dalton Trans.* 2020, **49**, 13693

50. M. Reigrotzki, H. Tsunetsugu, T.M. Rice, *J. Phys.-Cond. Matt.* 1994, **6**, 9235.

51. T. Barnes, E. Dagotto, J. Riera, E.S. Swanson, *Phys. Rev. B* 1993, **47**, 3196.

52. M. Greven, R.J. Birgeneau, U.J. Wiese, *Phys. Rev. Lett.* 1996, **77**, 1865.

53. S. Stoll, A. Schweiger, *J. Magn. Res.* 2006, **178**, 42.

54. P.A. Goddard, J. Singleton, P. Sengupta, R.D. McDonald, T. Lancaster, S.J. Blundell, F.L. Pratt, S. Cox, N. Harrison, J.L. Manson, H.I. Southerland, J.A. Schlueter, *New J. Phys.* 2008**, 10**, 083025.

55. J.L. Manson, M.M. Connor, J.A. Schlueter, A.C. McConnell, H.I. Southerland, I. Malfant, T. Lancaster, S.J. Blundell, M.L. Brooks, F.L. Pratt, J. Singleton, R.D. McDonald, C. Lee, M.-H. Whangbo, M.-H. *Chem. Mater.* 2008, **20**, 7408.

56. A.A. Validov, M. Ozerov, J. Wosnitza, S.A. Zvyagin, M.M. Turnbull, C.P. Landee, G.B. Teitel'baum, *J. Phys.-Cond. Matt.* 2014, **26**, 026003.

57. A. Bencini, D. Gatteschi. D. *EPR of Exchange Coupled Systsems*. Dover Publications, Inc.: Mineola, New York, 2012.

58. Crystallographic data might play a non-innocent role in determining the values of the critical field. See J. Jornet-Somoza, F. Cosi, M. Fumanal, M. Deumal, *Dalton Trans.* 2021, **50**, 1754.